Appl Biochem Biotechnol
DOI 10.1007/s12010-017-2549-6

Steered Molecular Dynamics for Investigating the Interactions Between Insulin Receptor Tyrosine Kinase (IRK) and Variants of Protein Tyrosine Phosphatase 1B (PTP1B)

Hung Nguyen[1] · **Nhat Do**[2] · **Tuyn Phan**[1] · **Tri Pham**[1]

Received: 22 March 2017 / Accepted: 25 June 2017

Abstract The aim of this study is to use steered molecular dynamics to investigate the dissociation process between IRK and PTP1Bs for wild type and five mutants (consisting of p.D181E, p.D181A, p.Q262A, p.D181A-Y46F, and p.D181A-Q262A). The gained results are observed not only the unbinding mechanism of IRK-PTP1B complexes came from pulling force profile, number of hydrogen bonds, and interaction energy between IRK and PTP1Bs but also described PTP1B's point mutations could variably change its binding affinity towards IRK. Additionally, the binding free energy calculated by Molecular Mechanics/Poisson-Boltzmann Surface Area (MM-PBSA) is also revealed that electrostatic energy and polar solvation energy mainly made up the binding free energy of PTP1B-IRK complexes.

Keywords SMD · IRK-PTP1Bs · MM-PBSA · Binding free energy

Introduction

Insulin resistance is characterized as attenuation of insulin action at the early step in signaling pathway [1]. Insulin action initiates at the insulin receptor (IR), a member of the receptor tyrosine kinase (RTK) family. IR consists of two extracellular α-subunits containing the insulin-binding sites and two transmembrane β-subunits possessing cytoplasmic tyrosine kinase domains, which form a disulfide-linked $\alpha_2\beta_2$ glycoprotein. The binding of insulin to the α chains induces structural changes within the receptor, resulting in ATP binding to intracellular components of the β subunit, whereby it facilitates auto-phosphorylation of

✉ Hung Nguyen
hung.nv@icst.org.vn

[1] Institute for Computational Science and Technology, Ho Chi Minh City, Vietnam

[2] Department of Medical Chemistry, Faculty of Pharmacy, University of Medicine and Pharmacy, Ho Chi Minh City, Vietnam

Published online: 13 July 2017

specific tyrosine residues, Tyr1158, Tyr1162, and Tyr1163, in the insulin receptor kinase (IRK) domain of the β chains. This triggers phosphorylation of insulin receptor substrates (IRS) that can then bind to other molecules to mediate the effects of insulin on cellular metabolism, growth, and glucose homeostasis [2–5]. The auto-phosphorylation and the activation of IRK play a crucial role in the transduction of most of the biological effects of insulin. Accordingly, crystal structures of IRK are determined in different states and in complex with substrates [6–8]. In the inactive, un-phosphorylated state, Tyr1162 serves as a "pseudosubstrate" which binds to the kinase active site, forming hydrogen bonds with Asp1132 and Arg1136 in the catalytic loop while residues in ^{1150}DFG motif of the activation loop occlude the ATP binding site in a form of an auto-inhibitory configuration [4, 7]. Upon insulin's binding to the IR, auto-phosphorylation of Tyr1158, Tyr1162, and Tyr1163 in the IRK domain causes a conformational change in the activation loop for the binding of ATP and protein substrates, thereby positioning residues, which is essential for catalysis [7].

The activated IR is regulated by dephosphorylation activity of several protein tyrosine phosphatases (PTPs). Among these PTPs, PTP1B is a prototypical protein and a highly specific negative regulator of the IR [9, 10]. Furthermore, prior animal studies revealed that elevated PTP1B activity and level could contribute to impaired glucose tolerance and insulin resistance in type 2 diabetes (T2D) while the lack of PTP1B gene could enhance insulin sensitivity [11–14]. Suppression of PTP1B to maintain the IRK in the active form may therefore be a potential strategy to treat T2D patients with insulin resistance. However, because PTP1B is involved in numerous signaling pathways, inhibition of IRK-PTP1B interaction is considered as an alternative strategy that has garnered much more attention of many researchers [15, 16].

Using in vitro methods like glutathione S-transferase fusion protein and scintillation proximity assay designed by Wang et al., previous studies revealed that PTP1B bound through its catalytic site to phosphorylated IR at phosphotyrosine residues [15, 17]. The specific interaction of PTP1B in a complex with mono-, bis-, and tris-phophorylated peptides derived from the activation segment sequence of the IR is also investigated by crystallographic and kinetic studies. The IRK peptides bind to the catalytic site of PTP1B; in which, the phosphotyrosine pTyr1162 interacts with residues of the PTP loop while pTyr1163 is located within a neighboring pTyr recognition site. Interestingly, the affinity of tandem pTyr-containing peptides for PTP1B is 70-fold greater than that of mono-pTyr peptides, indicating the importance of adjacent pTyr residues in PTP1B-IRK complex formation. Furthermore, from the structural data, the WPD loop (residues 179–185) undergoes a conformational change to cover the active site, creating a tight binding pocket for the substrate, representing a "closed" conformation upon substrate binding [18]. To analyze further the binding of IRK and PTP1B, the crystal structure at 2.3-Å resolution of a trapping mutant of the PTP1B catalytic domain and tris-(pTyr1158, pTyr1162, pTyr1163) phosphorylated IRK was determined. The striking feature of this structure was that instead of binding to a phosphotyrosine in the IRK activation loop, PTP1B targeted to the opposite side of the kinase domain through the key interaction Tyr152 and Tyr153 of PTP1B with the β2-β3 loop of IRK [6]. Although the crystal structure of the IRK-PTP1B complex was solved, it has remained unknown whether it is a stable conformation in physiological condition or just a non-catalytic binding mode due to impacts of ammonium sulfate in crystallization medium.

In recent studies, the effects of some PTP1B's mutations on substrate-binding characteristics of PTP1B have been reported. Some studies have mentioned that the PTP1B harboring p.D181E and p.D181A point mutations could exhibit a better binding affinity towards its

substrates. This can be attributed to D181 point mutations' ability to modify the nature of interactions between PTP1B binding site and PTP1B substrates, leading to an increase in binding affinity. More studies on the impact of D181 mutations are needed, but so far, the lack of X-ray crystal structures of D181 mutants has impeded further relevant studies [19, 20]. In an effort to investigate the effect of another mutation (p.Y46F) on the substrate trapping efficiency of classical PTP1B-D181A, Boubekeur S. et al. found that the double mutant PTP1B-D181A-Y46F could trap substrates more efficiently and precipitate a considerably higher amount of tyrosine-phosphorylated proteins than typical, commonly used D181A single mutant. Comparison between basal bioluminescence resonance energy transfer (BRET) and insulin-induced BRET signals in cells transfected with either PTP1B-D181A or PTP1B-D181A-Y46F showed that basal BRET was much higher in cells expressing PTP1B-D181A-Y46F while insulin-stimulated BRET dropped significantly with the Y46F mutant [21]. In another study, Xie L. et al. successfully generated PTP1B-D181A-Q262A which displayed more reduced catalytic activity and possessed further improved substrate-binding affinity than PTP1B-D181A. Moreover, PTP1B-D181A-Q262A could trap several new, less abundant tyrosine-phosphorylated proteins missed by PTP1B-D181A [22]. Basically, previous studies confirmed that PTP1B's point mutations (D181A, Y46F, and Q262A) played a crucial role in the binding mechanism of PTP1B-substrate complexes.

In this regard, we investigated the differences in kinetic and thermodynamic properties among IRK-PTP1Bs complexes (wild type and mutant forms) by use of the steered molecular dynamics. Also in this contribution, the free energies of IRK binding to wild-type and mutant PTP1Bs calculated by MM-PBSA are also presented in detail.

Materials and Methods

Materials

The 3D structure of wild-type PTP1B in complex with IRK was taken from the Protein Data Bank (PDB code 2B4S) [6]. Using the crystal structure of PTP1B, its mutants (p.D181E, p.D181A, p.Q262A, p.D181A-Y46F, and p.D181A-Q262A) were built via the mutagenesis tool integrated in visual molecular dynamics (VMD) [23]. These complexes' energies were minimized through 500,000 steps of steepest descent energy minimization followed by the classical atomistic molecular dynamic simulations using GROMACS 4.6.3 package [24]. Following the energy minimization process, 100 ps of position-restrained MD simulations was implemented to make water molecules enter the active site and the simulations started at 0 K and was heated up to 300 K over 500 ps. To make sure that the complex was stable, the system was equilibrated for 500 ps at 300 K in the NVT ensemble run with the Berendsen procedure [25]; and subsequently in 1000-ps NPT ensemble run at the pressure of 1 bar by use of the Parrinello-Rahman pressure coupling [26]. Finally, the dynamically equilibrated mutant structures were chosen before entering the steered molecular dynamic simulations.

Steered Molecular Dynamics

The steered molecular dynamics simulations of IRK-PTP1Bs complexes were performed with GROMOS 53A6 force field [27]. The IRK-PTP1Bs complexes were placed in a triclinic box of 10 nm × 8 nm × 16 nm to have enough space containing the IRK-PTP1Bs complex and pull

the IRK from the binding site of PTP1Bs in accordance with z-dimension, contained 39,501 SPC water molecules (Fig. 1) [28]. The three-dimensional coordinates of the center of the complex were 5, 4, and 5 nm. The complexes were immersed in a salt solution with a given concentration of 0.10 M of sodium and chloride, then sodium or chloride was added to neutralize the total charge of the proteins. The leap-frog algorithm [29] was used to integrate the equations of motion with the time step set to 2 femtosecond (fs). All chemical bonds within the protein were constrained using the Linear Constrain Solver (LINCS) algorithm [30]. The particle mesh Ewald truncation method [31] was used to treat the long-range electrostatic interactions. A van der Waals cutoff of 1.4 nm was used to depict non-bonded interactions. The non-bonded interaction pair-list was updated every 10 fs, using a cutoff of 1 nm. Although a virtual cantilever moving at the constant velocity v along the biggest z-axis of simulation box, the pulling force was applied to IRK's farthest peripheral atoms in the z-direction (Fig. 1). During the simulations, the spring constant k value was chosen as 600 kJ/(mol.nm^2) (approximately 1020 pN/nm). The disruption of hydrogen bonds between IRK and PTP1Bs is caused by the pulling force to move IRK. This total force could be measured by $F = k \times (vt - x)$, in which x accounted for the average shift of protein atoms from their initial locations. The complete disengagement of IRK from PTP1B's catalytic site was obtained through 1000-ps simulations with pulling velocity ranged by 19 values of v = 0.001, 0.0015, 0.002, 0.0025, 0.003, 0.0035, 0.004, 0.0045, 0.005, 0.0055, 0.006, 0.0065, 0.007, 0.0075, 0.008, 0.0085, 0.009, 0.0095, and 0.01 nm/ps. Then, the gained data from steered molecular dynamics (SMD) simulations are presented as the ensemble averaged results of 19 different simulation systems for each configuration.

Binding Free Energy Calculation Using MM-PBSA

We conducted atomistic MD simulations for 6 IRK-PTP1Bs complexes and used the Molecular Mechanics/Poisson-Boltzmann Surface Area (MM-PBSA) method [32–35] to calculate the binding free energies between IRK and PTP1Bs. Subsequently, snapshots of the simulation

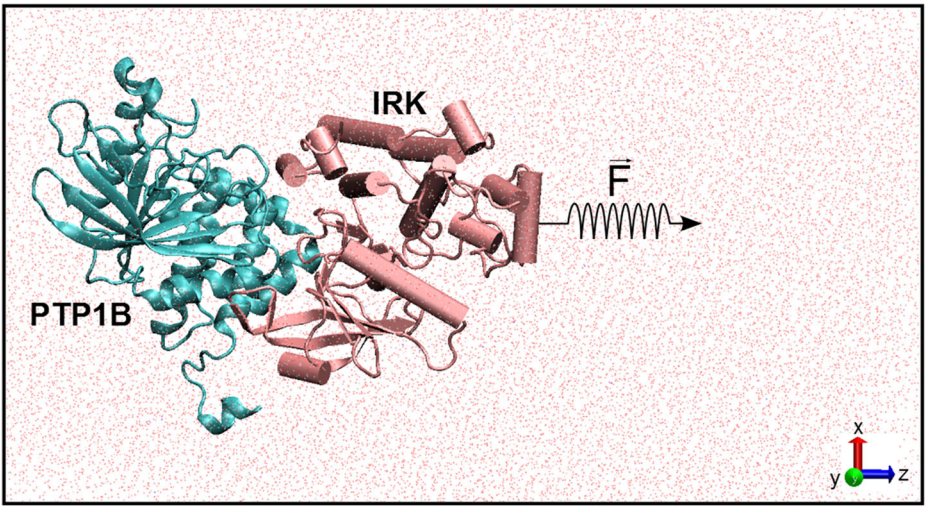

Fig. 1 Illustration of the IRK-PTP1B complex for SMD simulation

systems upon reaching dynamic equilibrium were used for binding free energy calculations. The MM-PBSA method was defined as follows:

$$\Delta G_{bind} = \Delta E_{elec} + \Delta E_{\mathrm{vdW}} + \Delta G_{\mathrm{sur}} + \Delta G_{\mathrm{PB}} - T\Delta S \quad (1)$$

Here, the ΔE_{elec} and ΔE_{vdW} were contributions from electrostatic and van der Waals (vdW) interactions. The G_{PB} was polar solvation energy determined by the continuum solvent approximation [36], which was the change of electrostatic interaction by transferring solute in a continuum medium from a low solute dielectric constant ($\varepsilon = 2$) to a higher one with water without salt ($\varepsilon = 78.45$).

The G_{sur} was non-polar solvation energy, which was approximated as linearly dependent on the solvent accessible method [37] in the APBS package [38]:

$$G_{\mathrm{sur}} = \gamma SASA + \beta \quad (2)$$

With $\gamma = 0.0072$ (kcal/mol) Å^2 and $\beta = 0$.

The entropy contribution ($T\Delta S$) was estimated from the average of 14 snapshots randomly collected from the last 7 ns of equilibrium MD trajectories. The simulation structures were minimized with no cutoff for non-bonded interactions by using the conjugate gradient and low memory Broyden-Fletcher-Goldfarb-Shanno method [39] until the maximum force was smaller than 10^{-6} kJ/(mol.nm). The conformational entropy of the solute S was estimated by normal mode analysis by diagonalizing the mass-weighted Hessian matrix [40]:

$$S = -R\ ln\left(\mathbf{1}-\boldsymbol{e}^{-\hbar\boldsymbol{v}_0/k_BT}\right) + \frac{N_A v_0 e^{-\hbar v_0/k_B T}}{T\left(1-e^{-\hbar v_0/k_B T}\right)} \quad (3)$$

Here, S was the vibrational entropy, $\hbar$ was Plank's constant, υ_0 was the frequency of the normal mode, k_{B} was the Boltzmann constant, T was 300 K, and N_{A} was Avogadro's number. We used the snapshots collected in the equilibrium of each system to calculate other terms of binding free energy.

Results and Discussion

To investigate the binding affinity and the impact of mutated residues in PTP1B structures through the interactions between IRK and PTP1Bs, the SMD simulation was used to probe the IRK-PTP1Bs complexes and pull the IRK away from the binding site of the PTP1Bs, whereby essential energy components involved in the unbinding processes were predicted. Here, the gained results will be presented as the ensemble averaged results of 19 different simulations for each complex.

As shown in Fig. 2, the pulling force profile reflected how pulling force values varied during the process of disengaging the IRK from the binding sites of the PTP1Bs. In detail, the pulling forces between the IRK and PTP1Bs grew larger and gained maximum force (F_{max}) around 400 ps for the wild type and p.D181A and p.Q262A and p. D181A-Y46F, 450 ps for p.D181E, and 500 ps for p.D181A-Q262A. At this point, the hydrogen bonds between the IRK and PTP1Bs started to break, which markedly lessened the IRK's affinity towards the

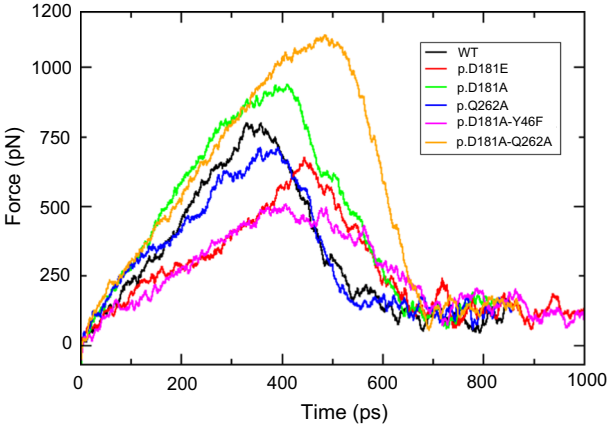

Fig. 2 Pulling force profiles for interaction process between the IRK and PTP1B variants

PTP1Bs. In the period from 350 to 550 ps, there are seen declines in the pulling forces as the number of hydrogen bonds continued to reduce and the IRK was slowly dissociated from PTP1Bs. From 700 ps onwards, the pulling forces have tended to fluctuate steadily between 100 and 250 pN as the IRK completely moved out from the PTP1Bs.

Also from this figure, the complex of the IRK and p.D181A-Q262A PTP1B is shown that its binding affinity is stronger than among the remaining complexes given with its largest pulling force ($F_{max} \approx 1115$ pN), which is even larger than from that of p.D181A-PTP1B ($F_{max} \approx 951$ pN) and is also noticeably larger than the pulling force obtained in the wild-type PTP1B ($F_{max} \approx 799$ pN), p.Q262A-PTP1B ($F_{max} \approx 710$ pN), p.D181E-PTP1B ($F_{max} \approx 674$ pN), and p.D181A-Y46F-PTP1B ($F_{max} \approx 509$ pN). In addition, the peaks' height in mutant cases is significantly different, implying that the forces required to split the complexes of the IRK and PTP1Bs mutants could be related to the break of hydrogen bonds between the IRK and PTP1Bs as well as the effects of the mutated residues to their binding affinity. The differences in magnitude of the pulling force along putative exit pathways among simulation complexes suggested a possibility of differences in their unbinding mechanisms. Overall, the variation of pulling force profiles among IRK-PTP1B complexes could attribute to the mutated residues at the binding site of PTP1Bs, and the mutated points might have changed hydrogen bonding network's properties and energy components in the IRK-PTP1Bs complexes led to alter the interactions between the IRK and PTP1Bs.

As seen from Fig. 3, the total number of hydrogen bonds (H-bonds) between the IRK and PTP1Bs is illustrated as a function of simulation time for all of the IRK-PTP1B complexes. Specifically, at the bound stage, the IRK interacted with PTP1Bs of the WT and p.Q262A and p.D181A-Y46F by mean of the H-bonds are fluctuated between 6 and 9 H-bonds, while the remaining complexes are established more than 12 H-bonds for the p.D181E and 15 H-bonds for the p.D181A and p.D181A-Q262A. Here, the H-bonds are decreased according to simulation time as the IRK is coming out from the binding pocket of the PTP1Bs. At the unbound stage, the H-bonds are approached to 0 H-bonds after a time of 700 ps for WT, around 750 ps for the p.Q262A and p.D181A, and around 900 ps for the p.D181A-Y46F and p.D181A-Q262A, while the H-bonds of p.D181E are still fluctuated around 5 H-bonds at 1000 ps. This is clear that the IRK came out from the binding pocket of the PTB1Bs but could still maintain some residual interactions with the PTP1Bs. In fact, at the rupture force values,

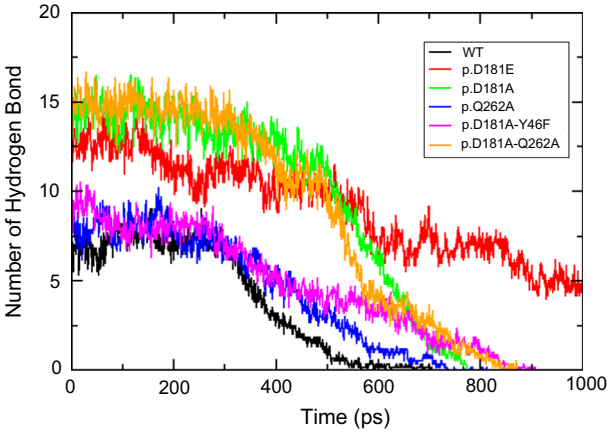

Fig. 3 The number of hydrogen bonds between the IRK and PTP1Bs of the complexes in relation to time

the H-bonds started to break as the IRK came out from the binding pocket of PTP1Bs, whereas the length of the peak in pulling force profiles is accounting still in the H-bonds established between IRK and PTP1Bs. Generally, the difference of the H-bonds established between IRK and PTP1Bs reflected the diverse effects that PTP1B's different point mutations imposed on the binding modes between IRK and PTP1Bs, leading to the increase of the H-bonds between IRK and PTP1Bs in the mutant variants. As a result, the contribution of the mutated residues plays an important role for the changes of the unbinding mechanism of the mutant complexes; this finding will be described more in detail in below parts.

To investigate the effect of mutated residues to the changes of binding affinity for the IRK-PTP1Bs complexes, the H-bonds formed between the mutated residue and its surrounding residues in the mutant variants are determined and compared with the H-bonds of the corresponding residue in the WT structure (Fig. 4). In detail, the first for the p.D181A and p.D181A-Y46F mutants, while the H-bonds of the mutated residue-Y46F are lost comparing to the H-bonds of residue-Y46 in the WT (Fig. 4b), the H-bonds formed between the mutated residue-D181A and its surrounding residues are increased in the p.D181A-Y46F and even stronger than those in p.D181A mutant (Fig. 4a). Thus, the loss of H-bonds of the mutated residue-Y46F and the increase of the H-bonds of the mutated residue-D181A for the p.D181A-Y46F and p.D181A mutants are caused for changing of the binding affinity comparing with the WT structure. The second for the p.D181A-Q262A and p.Q262A mutants, the archived result is easy to see that the loss of H-bonds of the mutated residue-Q262A and the increase of H-bonds of the mutated residue-D181A with its surrounding residues are necessary conditions to lead to the difference in unbinding mechanism in comparison to the WT structure. Finally, for the p.D181E mutant, the H-bonds formed between the mutated residue-D181E and its surrounding residues are larger than the H-bonds itself in the WT structure, even the H-bonds formed around mutated residue-D181E are also much more in comparison to those of the others. In summary, Asp 181 point mutations have tended to promote the increase of H-bonds while Gln 262 and Tyr 46 point mutations have tend to loss the H-bonds, which is compared with the gained results from the WT structure. As a result, the contribution of mutated residues is pretty much in control of the difference of the unbinding mechanism and binding free energy value of all the complexes, but it is not a decisive factor for the change of binding affinity between the IRK and PTP1Bs.

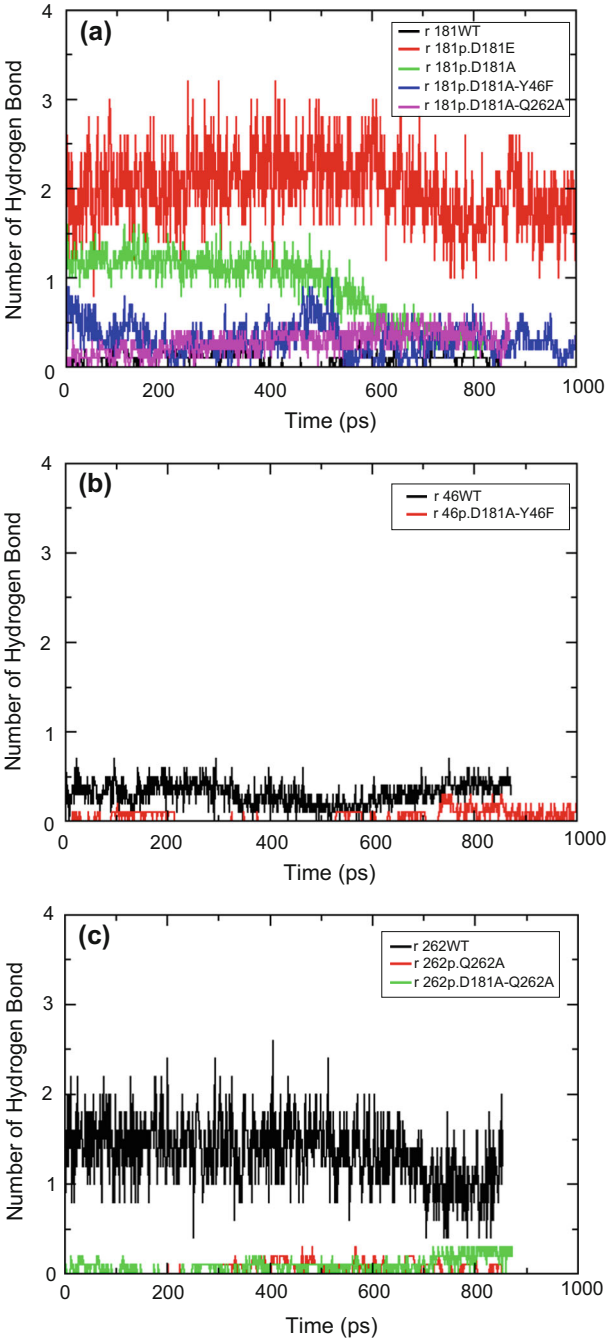

Fig. 4 The number of hydrogen bonds between mutated residues and its surrounding residues of mutant variants in comparison with WT as a function of simulation time

Figure 5 displays the van der Waals energy, electrostatic energy, and non-bonded interaction energy of IRK-PTP1Bs complexes in relation to time. Among these complexes, it

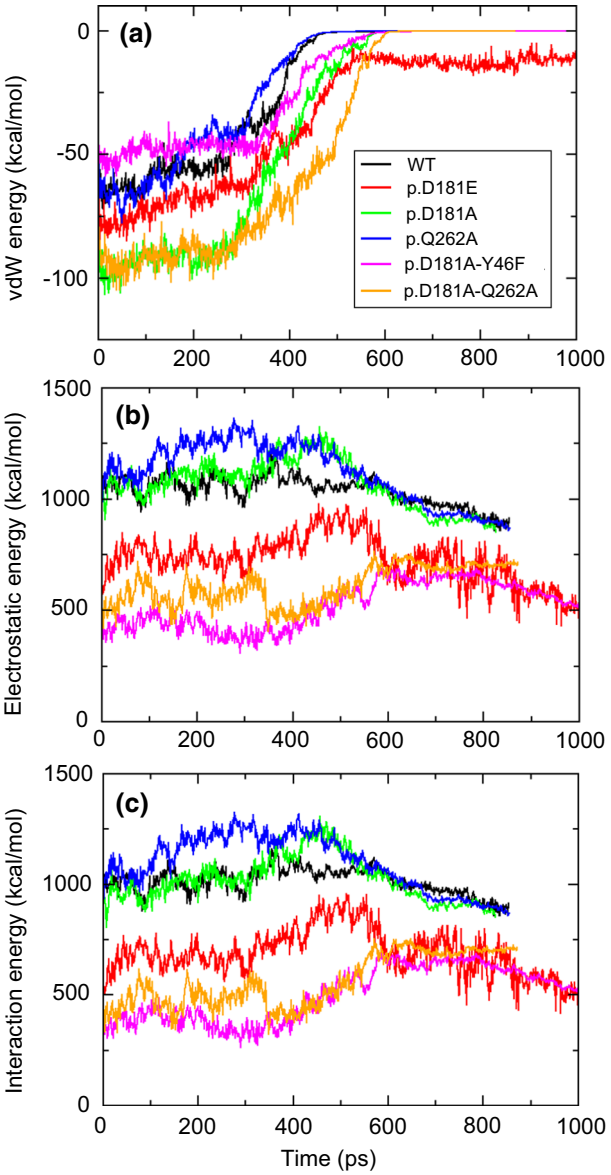

Fig. 5 Van der Waals energies, electrostatic energies, and interaction energies of IRK-PTP1Bs complexes in relation to time

could be realized that there are noticeable differences in electrostatic energy and non-bonded interaction energy while there are only slight differences in van der Waals energy. As non-bonded interactions composed of van der Waals and electrostatic energies, we presumed that the electrostatic energy for the IRK-PTP1B complexes accounts more for the differences in non-bonded interaction energy than the van der Waals energy between the wild-type and the mutant complexes. Moreover, the differences between graphic lines representing the interaction energies and electrostatic energies are not significant. This helped to reaffirm that the

electrostatic energy is mostly related to the interaction energy. In particular, at the beginning of SMD simulation, the vdW energy (Fig.5a) of all complexes is fluctuated around −50 kcal/mol for p.D181A-Y46F, around −65 kcal/mol for wild type and p.Q262A, around −75 kcal/mol for p.D181E, and around −90 kcal/mol for p.D181A and p.D181A-Q262A. Then, the vdW energies have come up to 0 kcal/mol after 500 ps for wild type and p.Q262A, after 600 ps for p.D181A and p.D181A-Y46F and p.D181A-Q262A, and is still not reaching to 0 kcal/mol at 1000 ps for p.D181E. The gained vdW value of p.D181E mutant has once again explained why the total number of hydrogen bonds of p.D181E mutant is larger than that of the others, although its pulling force profile is not outstanding. In contrast with the vdW energy, the electrostatic energies (Fig. 4b) of all complexes are differed remarkably in terms of maximum values and ranges. These energies exhibit an upward tendency in the beginning of the simulations, and then decrease over time. Specifically, at 0 ps, the electrostatic energies are fluctuated around 1150 kcal/mol for the wild type and p.Q262A and p.D181A, and fluctuated between 375 and 625 kcal/mol for p.D181E and p.D181A-Y46F and p.D181A-Q262A mutants. This difference perhaps is largely resulted from the fact that point mutations on PTP1B could redistribute charges on the complexes. The electrostatic energies of the p.D181A and p.Q262A mutants with positive charge of total charge 22 e and 23 lead to the emergence of repulsive interactions between IRK and mutant PTP1Bs, which ultimately decreased the binding affinity of the complexes as well as the generation of a much stronger binding than the other complexes (17 e for WT and p.D181A-Q262A, 19 e for p.D181E, and 15 e for p.D181A-Y46F). As a result, this data implied that substantial changes in the distribution of charge of the PTP1Bs generated significantly different results in the electrostatic energy profile by affecting strong Coulomb interactions. Moreover, the non-bonded interaction energy (Fig.5c) (sum of the vdW and electrostatic energies) also confirmed that the contribution of the electrostatic energy has a more key role than the H-bonds for the difference of the binding affinity between the WT and mutant variants.

The SMD, known as a method used to investigate unbinding process of a small molecule (IRK) to a large molecule (PTP1B), is capable of predicting relative binding affinity but cannot be used to calculate the absolute binding free energy. Overall, although the SMD method has provided good correlation with experimental results [41], their predictions are not always perfect. Therefore, the MM-PBSA method is then used to determine the binding free energies as an effort to elucidate the contribution of energy components in the interactions between the IRK and PTP1Bs. As seen in Table 1, the binding free energies are driven by electrostatic interaction and polar solvation while the vdW interaction and apolar solvation and entropy are directive, there is no significance for the differences of binding affinity between the IRK and PTP1Bs for the wild type and mutants. In more detail, the electrostatic and polar solvation energies vary substantially among complexes, which is ranged from −539.9 to −403.2 kcal/

Table 1 Binding free energies of IRK-PTP1Bs complexes determined using the MM-PBSA method (kcal/mol)

	ΔE_{elec}	ΔE_{vdW}	ΔG_{sur}	ΔG_{PB}	$-T\Delta S$	ΔG_{bind}
Wild type	−412.9	−48.9	−12.1	238.5	78.1	−157.3
p.D181E	−423.4	−56.0	−9.7	280.1	71.6	−137.4
p.D181A	−419.4	−84.4	−10.1	268.7	67.4	−177.8
p.Q262A	−539.9	−89.8	−13.0	405.4	76.2	−161.1
p.D181A-Y46F	−525.8	−50.5	−16.4	416.6	63.7	−112.4
p.D181A-Q262A	−403.2	−83.2	−12.9	228.2	76.6	−194.5

mol for electrostatic energy values, and ranged from 228.2 to 416.6 kcal/mol for polar solvation energy values. Moreover, almost, there is no considerable difference in the vdW interaction, apolar solvation, and entropy values among complexes. This is confirmed that the vdW energy and apolar solvation energy and entropy are not significantly contributed to the difference of binding free energy. Clearly, the gained values are ranged from −89.8 to −48.9 kcal/mol for the vdW energy, from −16.4 to −9.7 kcal/mol for the apolar solvation energy, and from 63.7 to 78.1 kcal/mol for entropy. Overall, the vdW energy and apolar solvation energy and entropy are distributed relatively equal among all complexes. Accordingly, it can be inferred that the difference in binding free energy values can be greatly attributed to the variations in the electrostatic energy and polar solvation energy values. This also means that the contribution of mutated residues not only is dominant to form hydrogen bonds but also depends on the electrostatic energy and polar solvation. In addition, Table 1 is also realized that the binding free energy of p.D181A-Q262A (−194.5 kcal/mol) is smaller than that of the other mutant complexes (−157.3, −137.4, −177.8, −161.1, and −112.4 kcal/mol). These data have led to the fact that the IRK expected to yield a more stable complex with the PTP1B-D181A-Q262A than with other PTP1Bs, and the additional Q262A mutation rendered the PTP1B-D181A more efficient in trapping high- and low-abundant PTP1B substrates. This finding agreed with the empirical results obtained from the study of Laiping Xie et al. [22].

Conclusions

In this work, we investigated the unbinding mechanisms and binding free energy of the IRK to PTP1B-substrates using the steered molecular dynamics and MM-PBSA method. The gained results come up with several observations:

1. The binding affinity between the IRK and PTP1Bs not only depended on the hydrogen bonds but also contributed from the strong electrostatic interactions of negatively charged residues at the active site of the PTP1Bs structures. Additionally, the gained result also confirmed that the electrostatic energy has a more important role than the vdW energy in investigating the unbinding mechanism of IRK-PTP1Bs complexes by use of the SMD simulation.
2. Point mutations in PTP1Bs are caused to lead to the changes in unbinding mechanisms determined by the SMD simulation as well as the binding free energy calculated by the MM-PBSA method for the IRK-PTP1Bs complexes. The MM-PBSA results revealed that electrostatic energy and polar solvation energy play important roles in constituting the binding free energy and are responsible for the difference in binding modes between IRK and PTB1Bs.
3. The results obtained by the MM-PBSA method are well agreeing with the SMD results and the prior publications. In recommendation, these complexes should be investigated for further studies in vitro and in vivo researches.

Acknowledgments The computing resources were provided by the Institute for Computational Science and Technology, Ho Chi Minh City, and are gratefully acknowledged. The authors would like to express their gratitude to Mr. Linh Nguyen for valuable advice.

Author Contributions Hung Nguyen designed the research, analyzed the data, and wrote the manuscript. Nhat Do and Tuyn Phan and Tri Pham analyzed the data. All authors reviewed the manuscript.

Compliance with Ethical Standards

Conflict of Interest The authors declare that they have no competing interests.

References

1. Olefsk, J. M. (1993). Insulin resistance and the pathogenesis of non-insulin dependent diabetes mellitus: cellular and molecular mechanisms. *Advances in Experimental Medicine and Biology, 334*, 129–150.
2. Wilcox, G. (2005). Insulin and insulin resistance. *The Clinical Biochemist Reviews, 26*, 19–39.
3. Kahn, C. R. (1994). Banting lecture. Insulin action, diabetogenes, and the cause of type II diabetes. *Diabetes, 43*, 1066–1084.
4. Hubbard, S. R. (2013). The insulin receptor: both a prototypical and atypical receptor tyrosine kinase. *Cold Spring Harbor Perspectives in Biology, 5*, a008946.
5. Kido, Y., Nakae, J., & Accili, D. (2001). Clinical review 125: the insulin receptor and its cellular targets. *The Journal of Clinical Endocrinology & Metabolism, 86*, 972–979.
6. Li, S., Depetris, R. S., Barford, D., Chernoff, J., & Hubbard, S. R. (2005). Crystal structure of a complex between protein tyrosine phosphatase 1B and the insulin receptor tyrosine kinase. *Structure, 13*, 1643–1651.
7. Hubbard, S. R. (1997). Crystal structure of the activated insulin receptor tyrosine kinase in complex with peptide substrate and ATP analog. *The EMBO Journal, 16*, 5572–5581.
8. Hubbard, S. R., Wei, L., Ellis, L., & Hendrickson, W. A. (1994). Crystal structure of the tyrosine kinase domain of the human insulin receptor. *Nature, 372*, 746–754.
9. Tonks, N. K. (2003). PTP1B: from the sidelines to the front lines! *FEBS Letters, 546*, 140–148.
10. Byon, J. C., Kusari, A. B., & Kusari, J. (1998). Protein-tyrosine phosphatase-1B acts as a negative regulator of insulin signal transduction. *Molecular and Cellular Biochemistry, 182*, 101–108.
11. Zabolotny, J. M., Haj, F. G., Kim, Y. B., Kim, H. J., Shulman, G. I., Kim, J. K., Neel, B. G., & Kahn, B. B. (2004). Transgenic overexpression of protein-tyrosine phosphatase 1B in muscle causes insulin resistance, but overexpression with leukocyte antigen-related phosphatase does not additively impair insulin action. *Jounal of Biological Chemistry, 279*, 24844–24851.
12. Ahmad, F., & Goldstein, B. J. (1995). Increased abundance of specific skeletal muscle protein-tyrosine phosphatases in a genetic model of insulin-resistant obesity and diabetes mellitus. *Metabolism, 44*, 1175–1184.
13. Dadke, S. S., Li, H. C., Kusari, A. B., Begum, N., & Kusari, J. (2000). Elevated expression and activity of protein-tyrosine phosphatase 1B in skeletal muscle of insulin-resistant type II diabetic Goto-Kakizaki rats. *Biochemical Biophysical Research Communications, 274*, 583–589.
14. Elchebly, M., Payette, P., Michaliszyn, E., Cromlish, W., Collins, S., Loy, A. L., Normandin, D., Cheng, A., Himms-Hagen, J., Chan, C. C., Ramachandran, C., Gresser, M. J., Tremblay, M. L., & Kennedy, B. P. (1999). Increased insulin sensitivity and obesity resistance in mice lacking the protein tyrosine phosphatase-1B gene. *Science, 283*, 1544–1548.
15. Wang, X. Y., Bergdahl, K., Heijbel, A., Liljebris, C., & Bleasdale, J. E. (2001). Analysis of in vitro interactions of protein tyrosine phosphatase 1B with insulin receptors. *Molecular and Celluler Endocrinology, 173*, 109–120.
16. Johnson, T. O., Ermolieff, J., & Jirousek, M. R. (2002). Protein tyrosine phosphatase 1B inhibitors for diabetes. *Nature Reviewer Drug Discovery, 1*, 696–709.
17. Seely, B. L., Staubs, P. A., Reichart, D. R., Berhanu, P., Milarski, K. L., Saltiel, A. R., Kusari, J., & Olefsky, J. M. (1996). Protein tyrosine phosphatase 1B interacts with the activated insulin receptor. *Diabetes, 45*, 1379–1385.
18. Salmeen, A., Andersen, J. N., Myers, M. P., Tonks, N. K., & Barford, D. (2000). Molecular basis for the dephosphorylation of the activation segment of the insulin receptor by protein tyrosine phosphatase 1B. *Molecular Cell, 6*, 1401–1412.
19. Flint, A. J., Tiganis, T., Barford, D., & Tonks, N. K. (1997). Development of "substratetrapping" mutants to identify physiological substrates of protein tyrosine phosphatases. *Proceedings of the National Academy of Science of the United State of America, 94*, 1680–1685.

20. Liu, M., Wang, L., Sun, X., & Zhao, X. (2014). Investigating the impact of Asp181 point mutations on interactions between PTP1B and Phosphotyrosine substrate. *Scientific Reports, 4*, 5095.
21. Boubekeur, S., Boute, N., Pagesy, P., Zilberfarb, V., Christeff, N., & Issad, T. (2011). A new highly efficient substrate-trapping mutant of protein tyrosine phosphatase IB (PTP1B) reveals full autoactivation of the insulin receptor precursor. *Journal of Biological Chemistry, 286*, 19373–19380.
22. Xie, L., Zhang, Y.-L., & Zhang, Z.-Y. (2002). Design and characterization of an improved protein tyrosine phosphatase substrate-trapping mutant. *Biochemistry, 41*, 4032–4039.
23. Humphrey, W., Dalke, A., & Schulten, K. (1996). VMD-visual molecular dynamics. *Molecular Graphics, 14*, 33–38.
24. Hess, B., Kutzner, C., Spoel, D., & Lindahl, E. (2008). GROMACS 4: algorithms for highly efficient, load-balanced, and scalable molecular simulation. *Journal of Chemical Theory and Computation, 4*, 435–447.
25. Berendsen, H. J. C., Postma, J. P. M., van Gunsteren, W. F., DiNola, A., & Haak, L. R. (1984). Molecular dynamics with coupling to an external bath. *The Journal of Chemical Physics, 81*, 3684–3690.
26. Parrinello, M., & Rahman, A. (1981). Polymorphic transitions in single crystals: a new molecular dynamics method. *Journal of Applied Physics, 52*, 7182–7190.
27. van Gunsteren, W. F., Billeter, S. R., Eising, A. A., Hünenberger, P. H., Krüger, P., Mark, A. E., Scott, W. R. P., & Tironi, I. G. (1996). *Biomolecular simulation: the GROMOS96 manual and userguide* (pp. 1–1042). Zurich: Vdf Hochschulverlag AG an der ETH Zurich.
28. Mark, P., & Nilsson, L. (2001). Structure and dynamics of the TIP3P, SPC, and SPC/E water models at 298 K. *The Journal of Physical Chemistry A, 105*, 9954–9960.
29. Hockney, R. W., Goel, S. P., & Eastwood, J. W. (1974). Quiet high-resolution computer models of a plasma. *Journal of Computational Physics, 14*, 148–158.
30. Hess, B., Bekker, H., Berendsen, H. J. C., & Fraaije, J. G. E. M. (1997). LINCS: a linear constraint solver for molecular simulations. *Journal of Computational Chemistry, 18*, 1463–1472.
31. Darden, T., York, D., & Pedersen, L. (1993). Particle mesh Ewald: an N-log(N) method for Ewald sums in large systems. *The Journal of Chemical Physics, 98*, 10089–10092.
32. Wang, J., Morin, P., Wang, W., & Kollman, P. A. (2001). Use of MM-PBSA in reproducing the binding free energies to HIV-1 RT of TIBO derivatives and predicting the binding mode to HIV-1 RT of efavirenz by docking and MM-PBSA. *Journal of the American Chemical Society, 123*, 5221–5230.
33. Nguyen, H., Nguyen, T., & Le, L. (2016). Computational study of glucose-6-phophate-dehydrogenase deficiencies using molecular dynamics simulation. *South Asian Journal of Life Sciences, 4*, 32–39.
34. Nguyen, H., & Le, L. (2015). Steered molecular dynamics approach for promising drugs for influenza A virus targeting channel proteins. *European Biophysics Journal, 44*, 447–455.
35. Nguyen, H., Tran, T., Fukunishi, Y., Higo, J., Nakamura, H., & Le, L. (2015). Computational study of drug binding affinity to influenza A neuraminidase using smooth reaction path generation (SRPG) method. *Journal of Chemical Information and Modeling, 55*, 1936–1943.
36. Sharp, K. A., & Honig, B. (1990). Electrostatic interactions in macromolecules: theory and applications. *Annual Review of Biophysics and Biophysical Chemistry, 19*, 301–332.
37. Shrake, A., & Rupley, J. A. (1973). Environment and exposure to solvent of protein atoms-lysozyme and insulin. *Journal of Molecular Biology, 79*, 351–371.
38. Baker, N. A., Sept, D., Joseph, S., Holst, M. J., & McCammon, J. A. (2001). Electrostatics of nanosystems: application to microtubules and the ribosome. *Proceedings of the National Academy of Science of the United State of America, 98*, 10037–10041.
39. Sitkoff, D., Sharp, K. A., & Honig, B. (1994). Accurate calculation of hydration free energies using macroscopic solvent models. *The Journal of Chemical Physics, 97*, 1978–1988.
40. Shanno, D. F. (1970). Conditioning of quasi-Newton methods for function minimization. *Mathematics of Computation, 24*, 647–656.
41. Li, M. S., & Mai, B. K. (2012). Steered molecular dynamics-a promising tool for drug design. *Current Bioinformatics, 7*, 342–351.